Determination of stellar parameters for FGK-dwarf stars: the NIR approach

by

Daniel Thaagaard Andreasen

A thesis submitted in conformity with the requirements
for the degree of Doctor of Philosophy
Graduate Department of Departamento de Fisica e Astronomia
University of Porto

Dedication

To Linnea, Henriette, and Rico

For always supporting me

Acknowledgements

Lorem ipsum dolor sit amet, consectetuer adipiscing elit. Ut purus elit, vestibulum ut, placerat ac, adipiscing vitae, felis. Curabitur dictum gravida mauris. Nam arcu libero, nonummy eget, consectetuer id, vulputate a, magna. Donec vehicula augue eu neque. Pellentesque habitant morbi tristique senectus et netus et malesuada fames ac turpis egestas. Mauris ut leo. Cras viverra metus rhoncus sem. Nulla et lectus vestibulum urna fringilla ultrices. Phasellus eu tellus sit amet tortor gravida placerat. Integer sapien est, iaculis in, pretium quis, viverra ac, nunc. Praesent eget sem vel leo ultrices bibendum. Aenean faucibus. Morbi dolor nulla, malesuada eu, pulvinar at, mollis ac, nulla. Curabitur auctor semper nulla. Donec varius orci eget risus. Duis nibh mi, congue eu, accumsan eleifend, sagittis quis, diam. Duis eget orci sit amet orci dignissim rutrum.

Nam dui ligula, fringilla a, euismod sodales, sollicitudin vel, wisi. Morbi auctor lorem non justo. Nam lacus libero, pretium at, lobortis vitae, ultricies et, tellus. Donec aliquet, tortor sed accumsan bibendum, erat ligula aliquet magna, vitae ornare odio metus a mi. Morbi ac orci et nisl hendrerit mollis. Suspendisse ut massa. Cras nec ante. Pellentesque a nulla. Cum sociis natoque penatibus et magnis dis parturient montes, nascetur ridiculus mus. Aliquam tincidunt urna. Nulla ullamcorper vestibulum turpis. Pellentesque cursus luctus mauris.

Abstract

Nam dui ligula, fringilla a, euismod sodales, sollicitudin vel, wisi. Morbi auctor lorem non justo. Nam lacus libero, pretium at, lobortis vitae, ultricies et, tellus. Donec aliquet, tortor sed accumsan bibendum, erat ligula aliquet magna, vitae ornare odio metus a mi. Morbi ac orci et nisl hendrerit mollis. Suspendisse ut massa. Cras nec ante. Pellentesque a nulla. Cum sociis natoque penatibus et magnis dis parturient montes, nascetur ridiculus mus. Aliquam tincidunt urna. Nulla ullamcorper vestibulum turpis. Pellentesque cursus luctus mauris.

Resumo

Nam dui ligula, fringilla a, euismod sodales, sollicitudin vel, wisi. Morbi auctor lorem non justo. Nam lacus libero, pretium at, lobortis vitae, ultricies et, tellus. Donec aliquet, tortor sed accumsan bibendum, erat ligula aliquet magna, vitae ornare odio metus a mi. Morbi ac orci et nisl hendrerit mollis. Suspendisse ut massa. Cras nec ante. Pellentesque a nulla. Cum sociis natoque penatibus et magnis dis parturient montes, nascetur ridiculus mus. Aliquam tincidunt urna. Nulla ullamcorper vestibulum turpis. Pellentesque cursus luctus mauris.

Contents

List of Tables

List of Figures

Chapter 4

Results for FGK stars

> Don't cry because it's over, smile because it happened.
>
> Dr. Seuss

It is time to apply the theory and methodology on some real data. In this chapter results from studies during the thesis will be presented. There is the analysis of three stars which lead to two papers, HD20010 (Andreasen et al., 2016) and Arcturus & 10 Leo (Andreasen et al., 2017a). A small summary of the stars and their characteristics can be found in Table 4.1. More details will be provided in the individual sections below for each star. An update to SWEET-Cat (Santos et al., 2013), a catalogue which provides homogeneous stellar parameters of planet hosts, was provided in Andreasen et al. (2017b). Additionally, there was an analysis of how a cut in excitation potential might affect the final parameters of a star. This will be discussed in Section 4.7, and last the analysis of a range of synthetic spectra from the PHOENIX spectral library (Husser et al., 2013), with $T_{\rm eff}$ lower than analysed in previous stars with the methodology described above in Section 3.3. However, before diving into the results of the analysis it is important to describe how the NIR line list was compiled, and why and how it was later refined.

Table 4.1: Summary of the four stars used in this thesis. The stellar parameters are from the PASTEL catalogue (Soubiran et al., 2016) (see text for details), except the parameters for the Sun.

Star	Spectrographs	Resolution	$T_{\rm eff}$ (K)	$\log g$ (dex)	$\xi_{\rm micro}$ (km/s)	[Fe/H] (dex)
Sun	FTS	600 000	5777	4.44	1.00	0.00
Arcturus	FTS	100 000	4300 ± 111	1.60 ± 0.29	1.93 ± 0.17	-0.54 ± 0.11
HD 20010	CRIRES	100 000	6152 ± 95	3.96 ± 0.11	1.17 ± 0.24	-0.27 ± 0.06
10 Leo	CRIRES	100 000	4742 ± 61	2.76 ± 0.17	1.45 ± 0.08	-0.03 ± 0.02

4.1 The creation of a NIR line list

As discussed extensively in Chapter 2 and Chapter 3, an atomic line list is needed for employing the method described here. This line list is made by neutral and ionized iron lines in the NIR. This has already been mentioned in Chapter 2. Here the process will be explained in greater detail below for the two versions presented in Andreasen et al. (2016) and Andreasen et al. (2017a), respectively.

4.1.1 First version

The first version of a NIR iron line list for determining stellar atmospheric parameters of high resolution and high S/N spectra were presented in Andreasen et al. (2016). Other NIR line lists exists such as the one from Lindgren et al. (2016); Önehag et al. (2012) for utilising the synthetic method described above. For this line list all iron transitions between 10 000 Å to 25 000 Å[1] were downloaded from the VALD database (Kupka et al., 2000; Piskunov et al., 1995). This only includes Fe I and Fe II transitions. In total were 50 198 Fe I and 28 339 Fe II lines respectively acquired.

Add more line lists from the literature.

The EW of all lines were measured in the solar atlas by Hinkle et al. (1995b). The EWs were measured using `ARES` due to the large amount of lines and to be as consistent as possible in the measurements. Since `ARES` expect a 1D spectrum with equidistant wavelength step, the solar spectrum was interpolated onto a regular wavelength grid of 0.01 Å. This did not change the appearance, and hence not the EW, of the final spectrum. This wavelength step is equivalent to a spectral resolution of 1 500 000 at 15 000 Å.

The EWs were measured by fitting Gaussian profiles to the spectral lines. For a given line, `ARES` output the central wavelength of the line (provided in the line list), the FWHM maximum of the fitted line, the number of lines fitted for the final result (in case of blending), the depth of the line, the EW of the line, and the Gaussian coefficients of the line. In the latest version of `ARES` , the error of the EW is also provided (Sousa et al., 2015).

Lines were discarded according to the following four criteria:

- Lines with EW lower than 5 mÅ as these lines can be problematic to see in spectra with lower S/N or spectra with many spectral features. Therefore the measurements of these lines are less reliable than stronger lines.
- Lines with EW higher than 200 mÅ as these lines are too strong to be fitted with a Gaussian profile. These lines might also be saturated and do not contain information about the abundance (see Figure 2.5).
- Lines where the total number of fitted lines are 10 or higher since they show indications of severe blending.
- If the fitted central wavelength is more than 0.05 Å away from the wavelength provided by VALD3 to avoid false identification. This should also remove some blended lines.

After this removal the number of Fe I and Fe II lines were reduced to 6060 and 2735, respectively.

4.1.1.1 Visual removal of lines

At this point a visual inspection were necessary. All absorption lines from all elements were downloaded from the VALD3 database in a 3 Å window around each of the nearly 9000 iron lines from the previous step. For each small spectral window, all absorption lines (including the iron line(s)) were plotted on top of the solar spectrum. An iron line was discarded if another line had the same central wavelength and/or the absorption line were severely blended. Most of the discarded iron lines had high EP, which are weak compared to the low EP lines. Therefore, it is fair to assume that many of these iron lines were falsely identified as another stronger line from another element. After the visual removal the number of Fe I and Fe II lines were reduced to a mere 593 and 22, respectively.

[1] That is equivalent to the YJHK bands.

For some of the absorption lines it was not clear which element was causing it. These lines were marked for further investigation with synthesis as described below.

4.1.1.2 Synthetic investigation

For the lines marked above for further investigation an even broader window were used of 6 Å. Once again, all lines were downloaded from the VALD3 database in these spectral windows. `MOOG` were used with the `synth` driver to create a synthetic spectrum using a solar atmosphere model with $T_{\rm eff} = 5777\,\mathrm{K}$, $\log g = 4.438$, $A(\mathrm{Fe}) = 7.47$, and $\xi_{\rm micro} = 1.00\,\mathrm{km/s}$. The iron abundance (7.47) is from Gonzalez and Laws (2000), while the overall metallicity for the solar atmosphere model is $[\mathrm{M}/\mathrm{H}] = 0.00$ by definition. This was done for all spectral windows for three different $[\mathrm{Fe}/\mathrm{H}] = \{-0.20; 0.00; 0.20\}$. Before creating a synthetic spectrum all elements which are more than singly ionised were removed since `MOOG` does not allow these. An example of the three synthetic spectra can be seen in Figure 4.1. Here the neutral iron line at 15 550.439 Å was investigated. The three coloured curves are synthetic spectra with the three different $[\mathrm{Fe}/\mathrm{H}]$. Note that while $[\mathrm{Fe}/\mathrm{H}]$ is used as a proxy for the over metallicity, $[\mathrm{M}/\mathrm{H}]$, it is here specific only the iron abundance that is changed. The upper plot shows the result with the full VALD3 line list, while in the lower plot the iron line were removed from the line list. In this case it is clear that the iron line is the cause of the absorption line. The grey curve is the solar atlas for reference. Note that it is not the purpose to match a synthetic spectrum to the solar atlas.

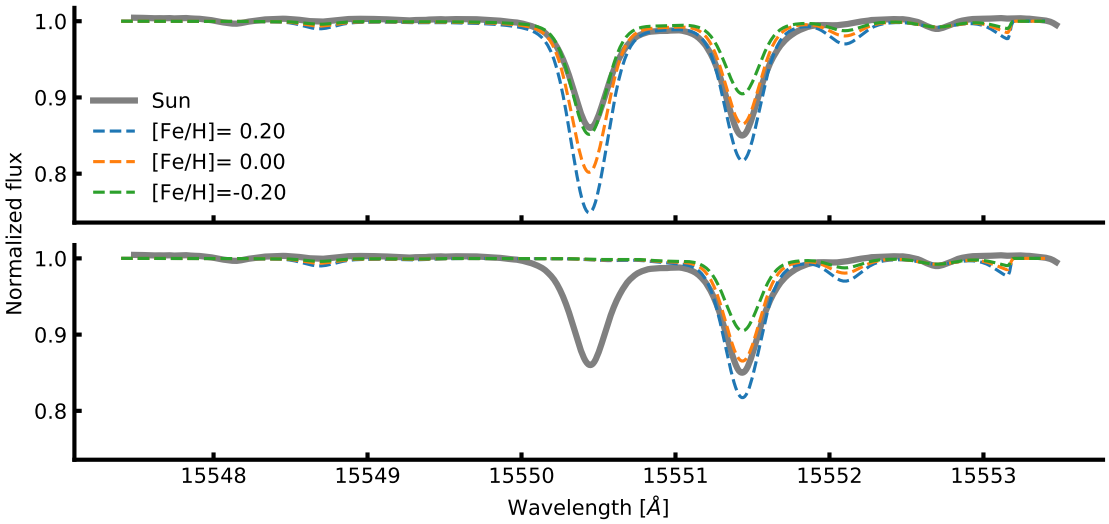

Figure 4.1: The three coloured curves represent different iron abundance, $\{-0.20; 0.00; 0.20\}$ compared to solar abundance. The grey curve is the solar atlas for reference. In this case the iron line at 15 550.439 Å was investigated. *Upper panel*: Synthetic spectra were computed using the full VALD line list in the spectral range for the three different iron abundances. *Lower panel*: Same as the upper panel, but with the iron line removed from the line list. Since the synthetic spectra shows no features at this absorption line anymore, it is a fair assumption to say the iron line is the cause of this absorption line.

If the three synthetic spectra shows variation at the iron line of interest, then it is assumed that the iron line is the cause for the absorption line. As a simple test, the iron line was also removed from the line list used to create the synthetic spectra. If the iron line in the synthetic spectra disappeared, it was a

clear signal that this line can be used in the final iron line list (this can be seen clearly in the lower plot of Figure 4.1). In some cases two iron lines had the same or very similar wavelength, and this technique was used to include the right iron line. In cases where both iron lines causes the absorption line, they were both discarded since they are blended.

In a few cases two iron lines had the same wavelength and EP but different $\log gf$. In these cases the two iron lines they can be combined into a single line by adding their gf values. After this step, there was 414 Fe I lines and 12 Fe II lines, respectively.

4.1.1.3 Calibrating the line list: astrophysical $\log gf$ values

These lines were collected into a single line list in the format required by MOOG (Sneden, 1973) and the line abundance were measured by all lines using the solar atmosphere model described above. If the derived abundance for a single line differs by more than 1.0 dex from the solar iron abundance, the line was discarded. The solar iron abundance used is 7.47 as found by Gonzalez and Laws (2000).

After the removal of the lines mentioned above, the final line list is almost compiled. At this point the line list has to be calibrated. This is done by changing $\log gf$ so the line abundance for all iron lines are 7.47 when using the solar atmosphere model mentioned above. As mentioned in Section 2.3 there is a anti-correlation between the abundance of a line and $\log gf$. This means a simple bisector minimization can be used to locate the $\log gf$ that gives the desired abundance. This was done for all the iron lines at this stage.

Note It is important to calibrate a line list if the setup of parameter determination is changed. This includes the type of model atmospheres used (e.g. ATLAS9 or MARCS), the interpolation code to generate a model atmosphere from the grid, or the settings of the radiative code, here `MOOG` . In the results listed below the setups are identical, except for the work done with synthetic spectra (see Section 4.5). There both ATLAS9 and MARCS model atmospheres were used, and a calibrated set of $\log gf$ values are available for both setups.

4.1.1.4 Removal of high dispersion lines

The line list calibrated above was used to derive parameters for HD 20010 (see Section 4.2), however the derived parameters showed poor results when compared to the literature values. This lead to the following test, where highly disperse lines would be removed.

A Gaussian distribution was made for the EW of each line centred on the EW itself,

$$f(x, EW, \sigma) = \frac{1}{\sqrt{2\pi\sigma^2}} e^{-\frac{(x-EW)^2}{2\sigma^2}}, \tag{4.1}$$

where σ is the error on the EW, expressed by Cayrel (1988):

$$\sigma \simeq 1.6 \frac{\sqrt{\Delta\lambda EW}}{S/N}, \tag{4.2}$$

where $\Delta\lambda = 0.1$ and a S/N=50 were considered here, which is much lower than the actual S/N of the solar atlas. 100 draws of the distribution above were made for each line and the abundances were derived using the solar atmosphere model. The mean absolute deviation (MAD) was calculated for each line abundance. The MAD for each line as a function of the original measured EW can be seen in Figure 4.2.

The trend for the weaker lines is expected since a small absolute change in the EW results in a large relative change in abundance. However, this does not mean these lines necessarily have a high dispersion. Therefore the disperse lines are found in the de-trended MAD value, where an exponential function was used for de-trending. A single point above 3σ was removed iteratively in the de-trended data. After this process there are 334 Fe I lines and 13 Fe II lines.

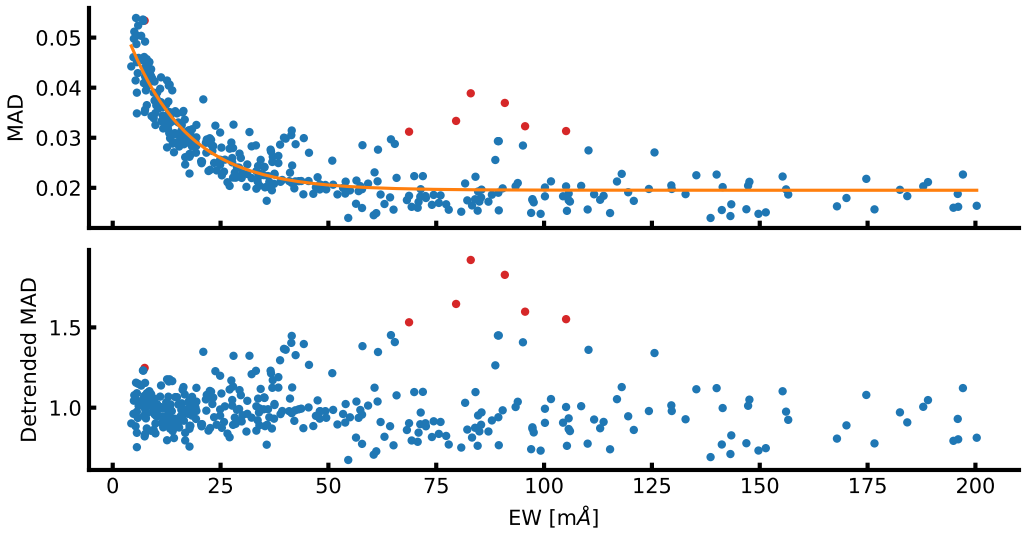

Figure 4.2: The most disperse lines. *Upper panel*: The MAD versus the original EW. The red points are the outliers which were discarded during this process. *Lower plot*: Same as above with the de-trended MAD by the exponential fit as shown in the upper panel.

4.1.2 Second version

As will be seen in Section 4.2.1 the line list presented above was used to derive atmospheric parameters of HD 20010. Even though the first test of the line list was success-full, it left room for improvements. The errors on the derived parameters were quite high for the spectral type compared results obtainable with a similar analysis utilising the optical spectrum (see Section 4.2.1 for details on this). Additionally, the derived metallicity was 0.10 dex higher than the literature values used.

If all derived parameters except metallicity are reliable (when compared to e.g. a literature value), then it suggest that the measured EW are either over- or underestimated. However, when using a line list for the first time like here, it can also suggest problems with the line list itself, most likely a bad calibration. This could have been wrong measurements of the EWs of the calibrator star, Sun in this case. This combines to several cases:

- Correct measurements of EWs of calibrator star:
  - Systematic lower measurements of EWs of target star leads to underestimated [M /H]
  - Systematic higher measurements of EWs of target star leads to overestimated [M /H]
  - Correct measurements of EWs of target star leads to correct [M /H]

- Systematic lower measurements of EWs of calibrator star:
  - Systematic lower measurements of EWs of target star leads to underestimated [M /H]
  - Systematic higher measurements of EWs of target star can lead to underestimated, correct or overestimated [M /H] depending on the amount of systematic higher measurements
  - Correct measurements of EWs of target star leads to underestimated [M /H]
- Systematic higher measurements of EWs of calibrator star:
  - Systematic lower measurements of EWs of target star can lead to overestimated, correct or underestimated [M /H] depending on the amount of systematic lower measurements
  - Systematic higher measurements of EWs of target star leads to overestimated [M /H]
  - Correct measurements of EWs of target star leads to overestimated [M /H]

It is important to note, that *correct* has been used here, assuming a perfect setup, that includes perfect model atmosphere, perfect radiative transfer code, etc. In reality the final [M /H] (and the other parameters) measured by different groups will occasionally differ regarding the setup used.

As described in Section 4.1.1 the EW of the Sun (calibrator star) was measured with `ARES` . A crucial option to set when using `ARES` is the `rejt` parameter as mentioned in Section 3.3.2. This option is used to place the continuum and will thus directly affect the measured EW. At the time of compiling the first version of the line list it seems the `rejt` value used did not reflect the high S/N of the spectrum, thus placing the continuum too low and thereby underestimate the EW.

In this second version of the line list, the goal is to:

1. Make sure the EW measurements are as correct as possible by measuring them by hand
2. Free of blended lines in cooler stars (K stars in this case)

The second point is a similar exercise which was done in the optical by Tsantaki et al. (2013), where blended lines were removed from the larger line list by Sousa et al. (2008). This allowed to determine the atmospheric parameters of stars colder than 5000 K. However, the optical spectrum still suffer for severely blended lines at low $T_{\rm eff}$, thus this method does not work for M stars.

Both of the above steps were done at the same time, by measuring the EWs by hand using `IRAF`. Whenever a line was difficult to reliably measure, i.e. a consistent measurement was not possible/easy, it was discarded since it was blended. This can be seen in Figure 4.3 where the EW measurements from the first version is shown against this version with the manual measurements. There are some measurements of EW higher than 150 mÅ which should have been removed. These lines have not been used during the analysis, however they were kept since they might appear useful on a later stage.

While the first version might seem careless since it is necessary with a second version, it is important to stress the 1) limited access on high quality of NIR spectra, and 2) the gained experience during the course of the thesis which proved valuable in the refining of the line list by a second visual inspection of the line list on the solar spectrum.

After the new measurements of the EWs, the line list was re-calibrated according to the procedure described above. The average change in $\log gf$ is -0.062 ± 0.157, i.e. on average the oscillator strengths are higher in the second version compared to the first version of the line list.

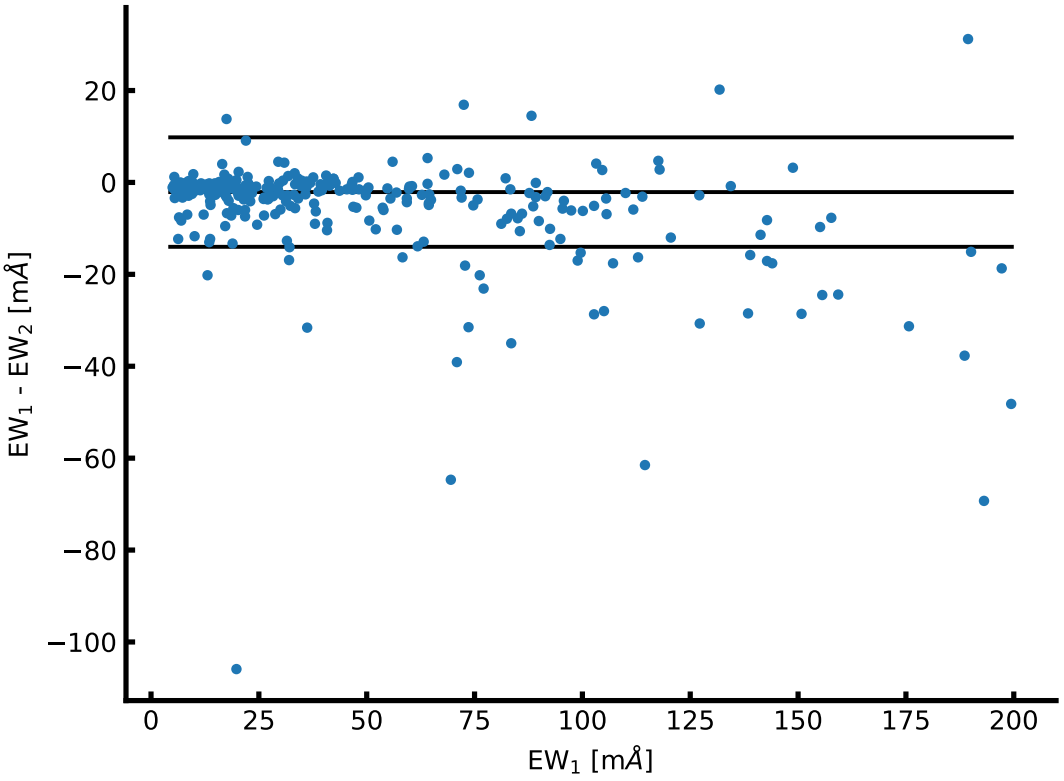

Figure 4.3: Comparison of the EW from the first version of the line list, EW_1, and the second version, EW_2. The EWs are generally higher in the second version, with an average difference between the two version of (2.1 ± 11.1) mÅ. The three horizontal lines show the average value and the standard deviation.

With the second version there are only 5 Fe II lines which is a concern since these are crucial for the derivation of the surface gravity. Therefore, when possible, it is important to obtain the $\log g$ from other more reliable studies.

4.2 HD20010

HD 20010 is a star that has been analysed twice with the methodology described here in this thesis. First time this star was analysed was in Andreasen et al. (2016) when the NIR line list was published (see Section 4.1.1). Later this line list was revised leading to a removal of several lines (see Section 4.1.2). This resulted in the second analysis in Andreasen et al. (2017a); both described below.

4.2.1 First analysis

To test the first version of the NIR line list a well-studied solar-type star was needed. The spectrum for such a target needs to be available in the NIR at both high resolution and high S/N. An ideal place to look for such a star was the CRIRES-POP database (Lebzelter et al., 2012b). Here, the best target for testing was HD 20010, an F8 subgiant star. At the time of writing this thesis and Andreasen et al. (2016) the spectrum of HD 20010 was not fully reduced. Here it is still contaminated by some telluric lines, and the wavelength solution used is not optimal. Both which are essential, however a tedious and difficult task to accomplish.

HD 20010 star has been part of many surveys and is therefore well studied. Different parameters from the literature are listed in Table 4.2.

Table 4.2: Selection of literature values for the atmospheric parameters for HD 20010. The mean and a 3σ standard deviation is presented at the end of the table from the literature values included, which was used as a reference for the derived parameters.

Author	$T_{\rm eff}$ (K)	$\log g$ (dex)	[Fe /H] (dex)	$\xi_{\rm micro}$ (km/s)
Balachandran (1990)	6152	4.15	-0.27 ± 0.08	1.60
Favata et al. (1997)	6000	...	-0.35 ± 0.07	...
Santos et al. (2004)	6275 ± 57	4.40 ± 0.37	-0.19 ± 0.06	2.41 ± 0.41
Gonzalez et al. (2010)	6170 ± 35	3.93 ± 0.02	-0.206 ± 0.025	1.70 ± 0.09
Ramírez et al. (2012)	6073 ± 78	3.91 ± 0.03	-0.30 ± 0.05	...
Mortier et al. (2013a)	6114	...	-0.19	...
Mean	6131 ± 255	4.01 ± 0.60	-0.23 ± 0.14	1.90 ± 1.08

The data available at CRIRES-POP are in the raw format and pipeline reduced, while three small pieces of the spectrum are fully reduced on the web page[2]. The data is in the standard CRIRES format with each fits file including four binary tables with the data from the four detectors. In the future, the final reduced data will be presented by the CRIRES-POP team. In contrast to the pipeline reduced data, this will be of higher quality, a better wavelength calibration, and telluric corrected.

The EWs were measured of the pipeline reduced spectrum, and where there was an overlap with the fully reduced spectrum, the EW was measured in both cases as a consistency check. The measured EWs from the fully reduced spectra were consistent with the measured EWs from the pipeline reduced spectra, although with less noise in the fully reduced spectral parts. As mentioned above, the Y, J, H,

[2] http://www.univie.ac.at/crirespop/data.htm

and K-bands, which are all available for this star, were used in this analysis. The spectra come in pieces of 50 Å to 120 Å. These pieces overlap each other, and up to five EW measurements were made for some lines. Unfortunately, wavelength calibration is a difficult task for CRIRES owing to the rather small spectral regions measured on each detector. Each calibration was performed separately for each detector and required the availability of a sufficient number of calibration lines in the respective spectral region. This was not always the case and a default linear solution was applied. A pipeline reduced spectrum shows up as a stretched spectrum if the wavelength calibration is poor compared to a model spectrum or a solar spectrum, for example. The wavelength calibration does not have any effect on the signal-to-noise ratio, which is generally high for the spectrum of HD 20010. The signal-to-noise varies between 200 and 400 for different chunks. However, the stretched spectra will most likely have an effect on the measured EWs.

The pipeline reduced spectrum for HD 20010 contains tellurics and the wavelength is shifted in radial velocity. All of these factors make the line identification very difficult, so a program was developed[3] to properly identify the lines, which does the following:

1. Plotting the observed spectrum
2. Overplotting a model spectrum. In this particular case the solar spectrum was used since the atmospheric parameters are close enough, so the sun was able to serve as a model
3. Overplotting a telluric spectrum from the TAPAS web page (Bertaux et al., 2014)
4. Overplotting vertical lines at the location of lines in the list
5. Calculating the cross-correlation function (CCF) for the telluric spectrum with respect to the observed spectrum, locating the maximum value by a Gaussian fit, and using this to shift the telluric spectrum with the found RV
6. Performing the same as step 5, but for the model spectrum
7. Shifting the lines with the same RV as found for the model/solar spectrum

The final plot shows the shifted spectra, and the CCFs at the sides. An example of the software in use is shown in . The two radial velocities (for the telluric and model spectrum) are part of the title of the plot. Once the lines were identified, the EWs were measured with the `splot` routine in *Image Reduction and Analysis Facility* (`IRAF`). The reason not to choose `ARES` for this task was to visually confirm the identification of the line given the relative poor wavelength calibration from the automatic pipeline. 249 Fe I lines and 5 Fe II EWs were measured compared to 344 Fe I lines and 13 Fe II lines for the Sun over the whole NIR spectral region in the first version of the line list. Whenever there were more than one EW measurement of a line, the average was used for the final EW. The stellar atmospheric parameters were derived using the standard procedure (see Section 3.3). Lines below 5 mÅ were removed in order to remove the lines which are most affected by contamination from either telluric or other line blends. Additionally, a cut in EP at 5.5 eV was made since the Fe I and Fe II lines usually used for stellar parameter determination in the optical regime are also limited to similar values (see e.g Sousa et al., 2008). Higher excitation potential lines are also more likely to be affected by non-LTE effects.

Make a plot of this

[3] The program (and other small scripts) can be found herehttps://github.com/DanielAndreasen/astro_scripts

The parameters were derived with one outlier in abundance removed iteratively (after a completed minimization) until no outliers were present. Since we could only measure 5 Fe II lines, the parameter were also derived with $\log g = 4.01$ dex fixed at the reference mean value (see Table 4.2). The resulting atmospheric parameters and iron abundances are presented in Table 4.3. The effective temperature, surface gravity, and metallicity agree within the errors with the literature values. Similar parameters are obtained by fixing $\log g$ to the average literature value or by leaving it free.

Table 4.3: The derived parameters for HD20010 with and without fixed surface gravity.

	$T_{\rm eff}$ (K)	$\log g$ (dex)	$\xi_{\rm micro}$ (km/s)	[Fe/H] (dex)
Literature	6131 ± 255	4.01 ± 0.60	1.90 ± 1.08	-0.23 ± 0.14
	6116 ± 224	4.21 ± 0.58	2.45 ± 0.45	-0.14 ± 0.14
	6144 ± 212	4.01 (fixed)	2.66 ± 0.42	-0.13 ± 0.29

The errors on the atmospheric parameters for HD 20010 are much higher than what is achievable with other measurements in the literature, as presented above in Table 4.2. In order to explain these errors, the abundances for all lines which have at least two measurements of the EW were calculated from the highest and lowest measured EW. The differences in abundances are presented in Figure 4.4. The very large differences (more than 0.1 dex) translate to the high errors in the parameters.

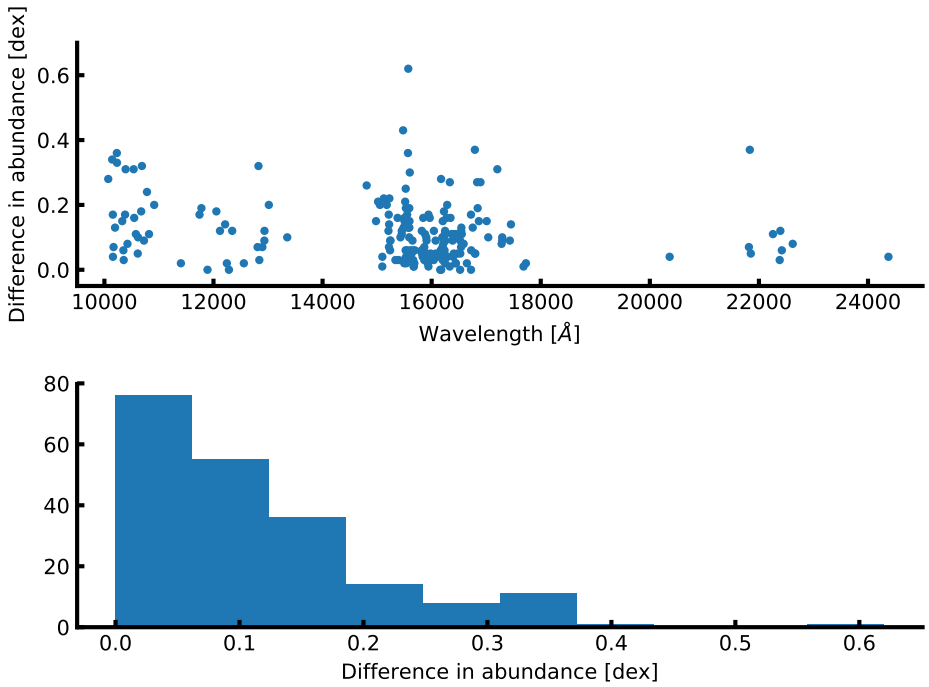

Figure 4.4: Difference in abundance for HD 20010 when multiple measurements of EW were obtained. The differences are between the lowest and highest measured EW in case of multiple measurements. This is shown against the wavelength (*upper panel*) and in a histogram (*lower panel*).

This test strongly suggest that errors in the EWs, likely due to the telluric contamination and non-optimal reduction of the spectrum (poor default wavelength calibration), are responsible for the relatively large error in the derived stellar parameters. After the first analysis of HD 20010, the CRIRES-POP

team published a fully reduced spectrum of 10 Leo (Nicholls et al., 2017) with telluric correction and an optimal wavelength solution. The results obtained from this star (see Section 4.4) are very promising for the method used here, and it encourage a complete re-visit of HD 20010 once the reduction is optimal.

4.2.2 Second analysis

During the analysis of Arcturus (see Section 4.3) and 10 Leo (see Section 4.4) with the refined line list presented in Section 4.1.2 it was a simple task to apply the updated line list on HD 20010 a second time as a test whether it would perform similar, worse or better. This is compared to results obtained from the literature and the previous results in Section 4.2.1.

Therefore HD 20010 was revisited, and the atmospheric stellar parameters were derived. The measured EWs from the results above in Section 4.2.1 were kept, however the lines which did not make the cut in the second version of the line list were removed. Moreover, the $\log gf$ values were updated since these were re-calibrated.

`FASMA` was used to obtain the results which are shown in Table 4.4 along with the results for Arcturus and 10 Leo (details on their parameters will be found below). The agreement with the adopted average literature values are better for HD 20010 compared to the results from above in Section 4.2.1 (especially [Fe /H] and $\log g$), and smaller errors with the updated results. This first test of the line list already shows promising results. The literature values are slightly different here than compared to the first analysis of this star. This is solely because other references were used, the PASTEL catalogue (Soubiran et al., 2016). However, this does not change the improvement seen.

Table 4.4: Results for the three stars where first set of parameters are the literature values as presented in Table 4.1, second set of parameters are results with $\log g$ set to the same value during the minimization procedure as found in the literature (fixed), and last set of parameters are with all parameters free during the minimization procedure.

	HD 20010	10 Leo	Arcturus
Literature			
$T_{\rm eff}$ (lit.)	6152 ± 95	4741 ± 60	4300 ± 110
$\log g$ (lit.)	3.96 ± 0.19	2.76 ± 0.17	1.60 ± 0.29
[Fe /H] (lit.)	-0.27 ± 0.06	-0.03 ± 0.02	-0.54 ± 0.11
$\xi_{\rm micro}$ (lit.)	1.17 ± 0.24	1.45 ± 0.08	1.93 ± 0.13
$\log g$ fixed			
$T_{\rm eff}$	6161 ± 164	4761 ± 118	4357 ± 74
$\log g$	3.96 (fixed)	2.76 (fixed)	1.60 (fixed)
[Fe /H]	-0.18 ± 0.11	0.01 ± 0.07	-0.55 ± 0.04
$\xi_{\rm micro}$	1.72 ± 0.44	1.25 ± 0.11	1.55 ± 0.10
All free			
$T_{\rm eff}$	6162 ± 184	4805 ± 98	4439 ± 62
$\log g$	4.08 ± 0.77	2.42 ± 0.61	1.20 ± 0.20
[Fe /H]	-0.18 ± 0.11	-0.01 ± 0.07	-0.58 ± 0.06
$\xi_{\rm micro}$	1.59 ± 0.49	1.23 ± 0.10	1.55 ± 0.10

4.3 Arcturus

Arcturus is one of the brightest stars on the Northern hemisphere with a V magnitude of -0.05 (Ducati, 2002), and is well studied (see e.g. Griffin and Griffin, 1967; McWilliam, 1990; Ramírez et al., 2013, to mention just a few), and a benchmark star in current spectroscopic surveys such as Gaia-ESO (Jofré et al., 2014; Smiljanic et al., 2014). Hence it is a prime target for testing with the numerous measurements of the atmospheric parameters.

Use benchmark parameters instead of PASTEL!

The atlas of Arcturus, acquired at Kitt Peak National Observatory using the FTS spectrograph at the Mayall telescope by Hinkle et al. (1995a), covers the spectral range of interest (YJHK bands). Strong telluric features were identified with a spectrum from the TAPAS web page (Bertaux et al., 2014) which was useful during the line identification. The atlas also comes with a telluric standard and the ratio of the two spectra in order to correct for the tellurics. The telluric spectrum from TAPAS was only used for telluric line identification. Both the telluric corrected and non-corrected spectra was used during the analysis, however the focus was on the non-corrected spectrum since it is simple to identify the telluric lines in this spectrum.

The atlas consists of both a summer observation set and a winter observation set. The two data sets have been obtained in order to minimise the effect of tellurics at different spectral regions. A comparison between the two sets of measured EWs, both the manual measurements using `IRAF` and the automatic measurements using `ARES` , are shown in Figure 4.5. The automatic EW measurements for the summer set and winter set show excellent agreement with a dispersion of 7 mÅ. This means that the two data sets are very similar, thus it was decided to only manually measure the EWs for one set (summer). Since the EWs are very similar the parameters are only derived from from the summer set with the EWs measured by `ARES` . Parameters were derived with and without $\log g$ set to a fixed value (1.60 dex, the average literature value adopted). The derivation of the parameters followed the same procedure as described above for HD 20010 using `FASMA` . Again outliers in abundance were removed one at the time until there were no more outliers. The final results are presented in Table 4.4 together with mean parameters from the literature.

There is overall good agreement between the derived parameters and the average values from the literature adopted (see Table 4.4). The only parameter being difficult to measure is the surface gravity due to the low number of Fe II lines in the NIR. This was already suspected and mentioned in Section 4.1.2. There are also some problems determining $\xi_{\rm micro}$, however this is not a major concern, since it is not as important a parameter as the other three. The derived metallicity is consistent with the literature here which is promising since there were some problems with this parameter in Section 4.2.1.

4.4 10 Leo

The spectrum for 10 Leo was made available by the CRIRES-POP team (Nicholls et al., 2017). 10 Leo is very similar to Arcturus, which is also one reason this star was the first to be fully reduced by the CRIRES-POP team. The spectrum is divided into several pieces according to the atmospheric windows in the NIR: YJ (only together), H, K, L, and M. Here the first three were used since this is the range of the line list. Some small gaps are present in the spectrum due to tellurics that could not be properly removed, low S/N, bad pixels, etc. Rather than giving an uncertain interpolation, Nicholls et al. (2017) decided to leave small gaps in the data. This had very little effect on this line by line analysis, however,

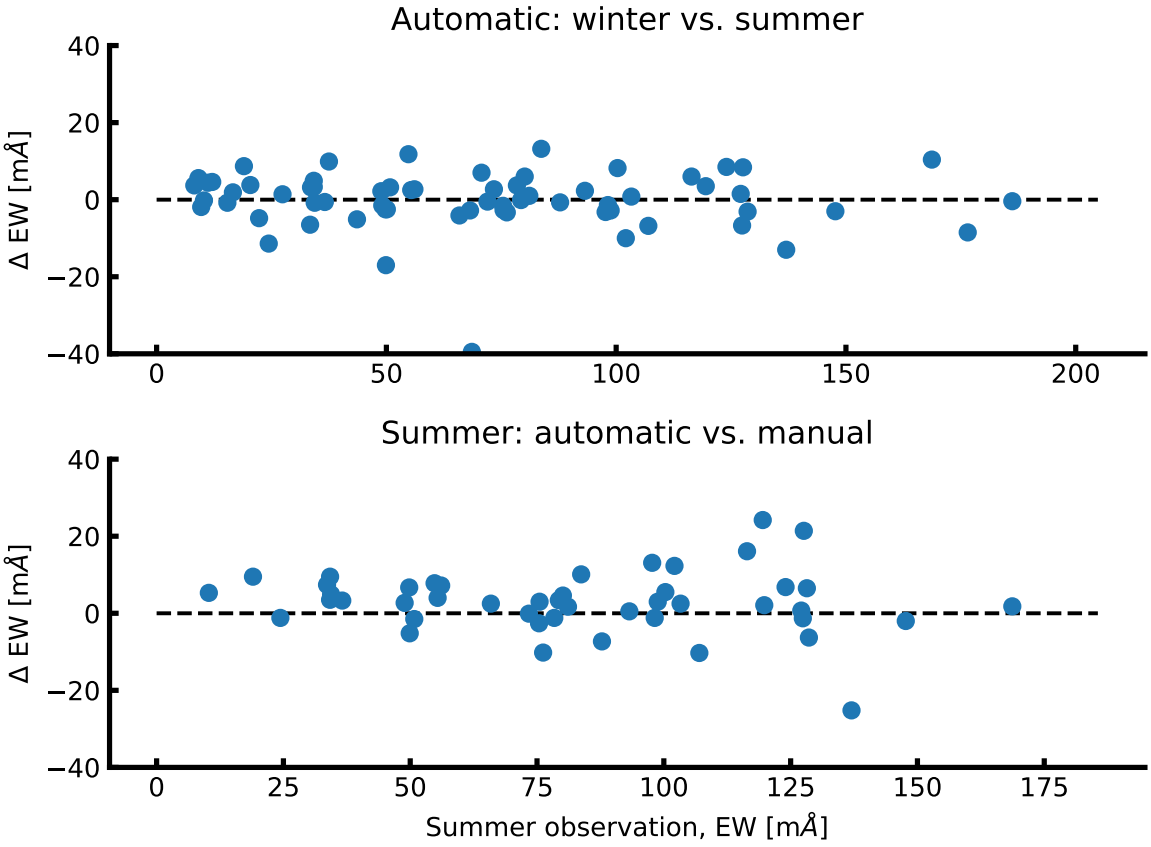

Figure 4.5: Top figure: Difference of the automatic EW measurements between the summer observations and winter observations from the Arcturus spectra. Bottom figure: Same as above, but with manual measurements from ARES (summer) and automatic measurements (summer).

due to those gaps, one Fe II line were not measured which are crucial to determine the surface gravity.

The approach for determining the atmospheric stellar parameters for 10 Leo is identical to Arcturus. ARES was used on each band (YJ, H, and K-band) separately. For the small gaps in the spectrum, the flux was simply set to 1, since the spectrum has already been normalised. This also prevented ARES to identify and measure any lines in these regions. The EWs from the three regions were combined to one final line list used for the determination of the parameters. The final results can be seen in Table 4.4.

Generally the derived parameters are in excellent agreement with the literature values listed here. A 64 K difference is seen for $T_{\rm eff}$ with $\log g$ set as a free parameter, well within the errors. The only parameter that show a discrepancy compared to the literature value is $\xi_{\rm micro}$ with a difference of 0.22 km/s, which is at the limit of the errors reported. We note that this parameter is not reported in the PASTEL database, and this was a derived parameter from an empirical relation. $\log g$ was derived with large errors which is a result from the few Fe II (three lines) measured. However, the $\log g$ is not far from the literature value, only 0.34 dex lower, which is well within the large errors reported. However, it also shows it is safer to obtain $\log g$ from other more reliable methods, such as asteroseismology when possible.

Then find some reliable values instead

4.5 Synthetic cool stars

Mainly due to lack of available high quality spectra in the NIR, it is a good test to do a simulation. By deriving parameters from synthetic spectra, it is possible to carefully control the work flow, in the sense that the target parameters are known. In this section the synthetic library[4] by Husser et al. (2013) will be used. For this test only the $T_{\rm eff}$ will vary, ranging from 3500 K to 6000 K with most densely sampled at lower temperatures (see Figure 4.7). Here $\log g = 4.5$ dex and $[{\rm M}/{\rm H}] = 0.00$ dex, i.e. synthesised dwarf stars with solar metallicity.

Did not mention the broadening of the spectra yet...

In this test ARES was used to measure the EWs of as many lines from the line list (second version) as possible for each of the 12 synthetic spectra. These line list were used to derive parameters with two different model atmospheres, ATLAS9 (Kurucz, 1993) and MARCS (Gustafsson et al., 2008), with FASMA . This was done twice, with all parameters derived from FASMA (Figure 4.7), and again with $\log g$ fixed at 4.5 dex and $\xi_{\rm micro}$ fixed which means it is changed in each iteration (see Section 3.3 for details) according to an empirical relation. The latter case with fixed parameters is shown in Figure 4.6.

For the results with $\log g$ and $\xi_{\rm micro}$ fixed at the correct parameters during the derivation, the first thing noticed is the well agreement between the two model atmospheres. Second, the derived $T_{\rm eff}$ are underestimated for $T_{\rm eff} > 4000$ K while for the two lowest $T_{\rm eff}$ it is the opposite case. It is important to know that the grid of ATLAS9 models only go down to 3750 K, however these synthetic spectra were included for completeness. In this case the mean metallicity for the 12 synthetic spectra are $[{\rm Fe}/{\rm H}] = (-0.12 \pm 0.17)$ dex and $[{\rm Fe}/{\rm H}] = (-0.19 \pm 0.12)$ dex for the ATLAS9 and MARCS model atmospheres, respectively.

When all the parameters are derived it is a very different story for $T_{\rm eff}$. In this case the $T_{\rm eff}$ are overestimated for the synthetic spectra colder than 5000 K. Above this limit the $T_{\rm eff}$ are slightly underestimated with a hint of the results getting worse further from this limit. The reason for this can partly be found in the measured Fe II lines. As mentioned before, these are used to determine $\log g$. There have been measured between 1 and 3 Fe II lines, generally fewer the lower $T_{\rm eff}$ is, out of 5 possible measurements. The mean derived values for the surface gravity are $\log g = (1.11 \pm 1.63)$ dex and

[4] http://phoenix.astro.physik.uni-goettingen.de/

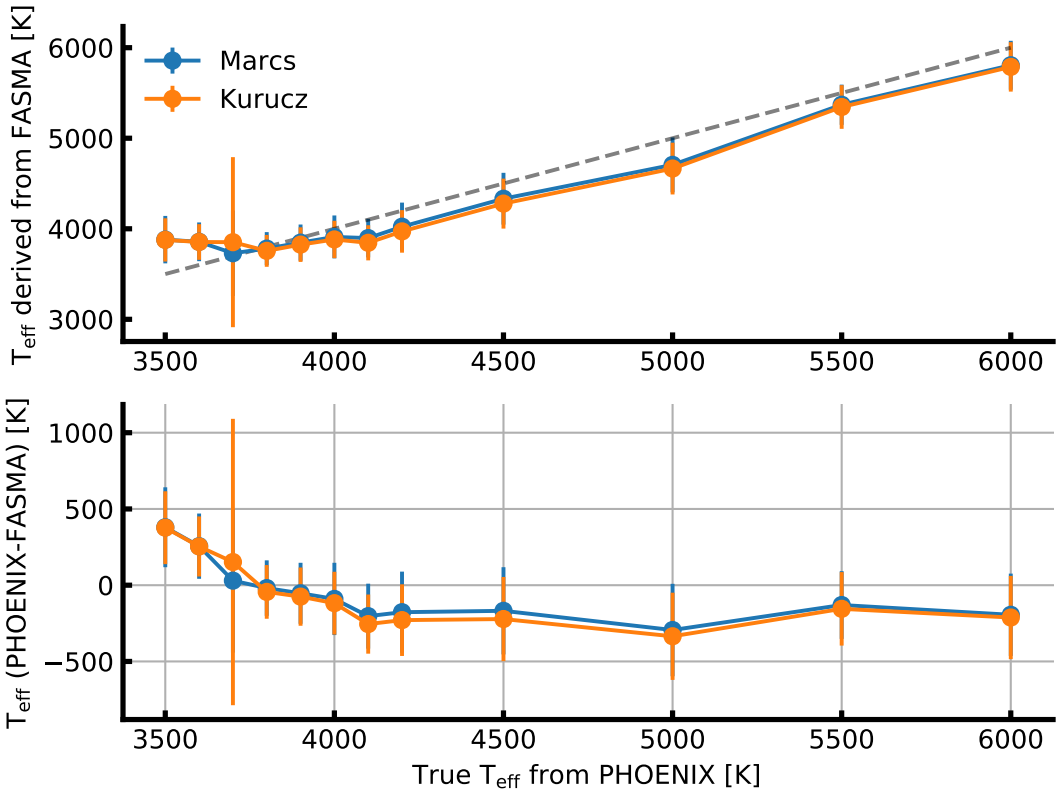

Figure 4.6: Derived parameters of 12 synthetic PHOENIX spectra with varying $T_{\rm eff}$. Here $\log g$ is fixed at 4.5 dex and $\xi_{\rm micro}$ fixed according to an empirical relation, thus only deriving $T_{\rm eff}$ and [Fe / H].

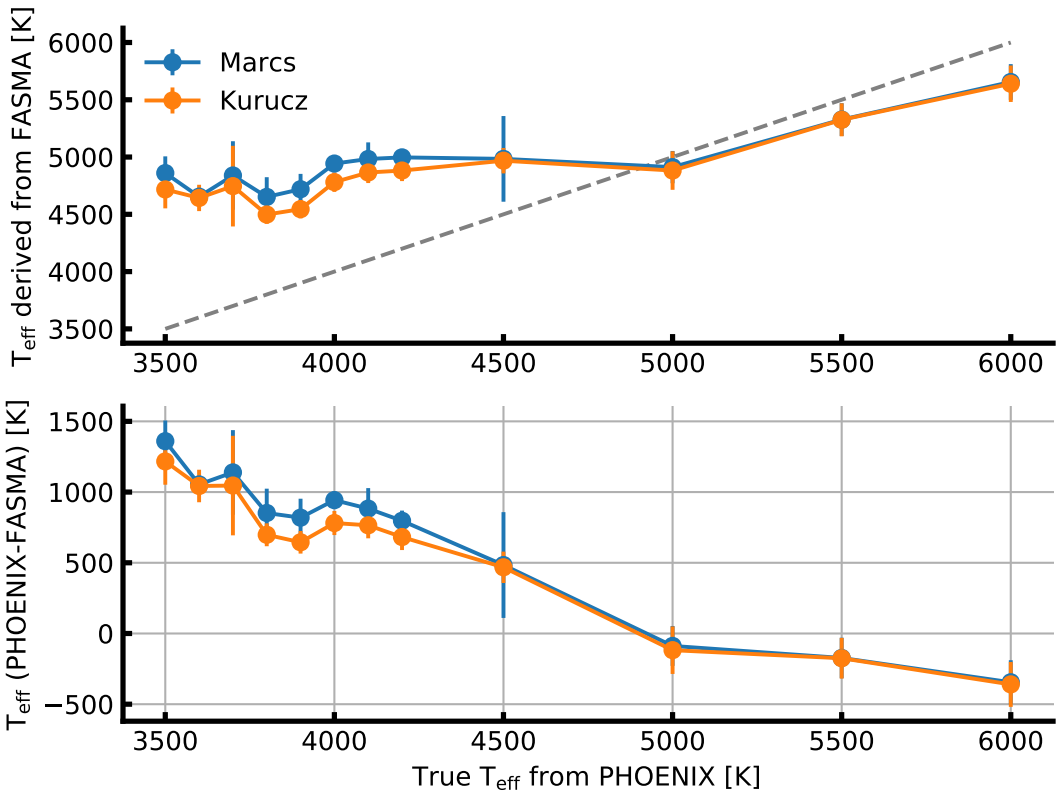

Figure 4.7: Same as Figure 4.6 but with all parameters derived.

$\log g = (1.38 \pm 1.45)$ dex for ATLAS9 and MARCS model atmospheres, respectively. Similarly for the metallicity the following mean values are $[\mathrm{Fe}/\mathrm{H}] = (-0.73 \pm 0.37)$ dex and $[\mathrm{Fe}/\mathrm{H}] = (-0.73 \pm 0.38)$ dex for ATLAS9 and MARCS model atmospheres, respectively.

Another cause for the differences found in the parameters can be found in the synthetic spectra themselves. In Figure 4.8 a PHOENIX synthetic spectrum with $T_{\mathrm{eff}} = 4300$ K, $\log g = 1.50$ dex, and $[\mathrm{Fe}/\mathrm{H}] = -0.50$ dex is plotted with a piece of the Arcturus atlas from Section 4.3. The synthetic spectrum has similar parameters as Arcturus, thus they should have similar spectral features. However, in the plot the spectral lines are deeper for the PHOENIX model and there seem to be more absorption lines in this synthetic spectrum compared to the observed spectrum. This have a direct effect on the measured EWs as they will be blended and deeper than expected.

Does this improve if the synthetic spectrum is broadened to same R as Arcturus? Probably not much...

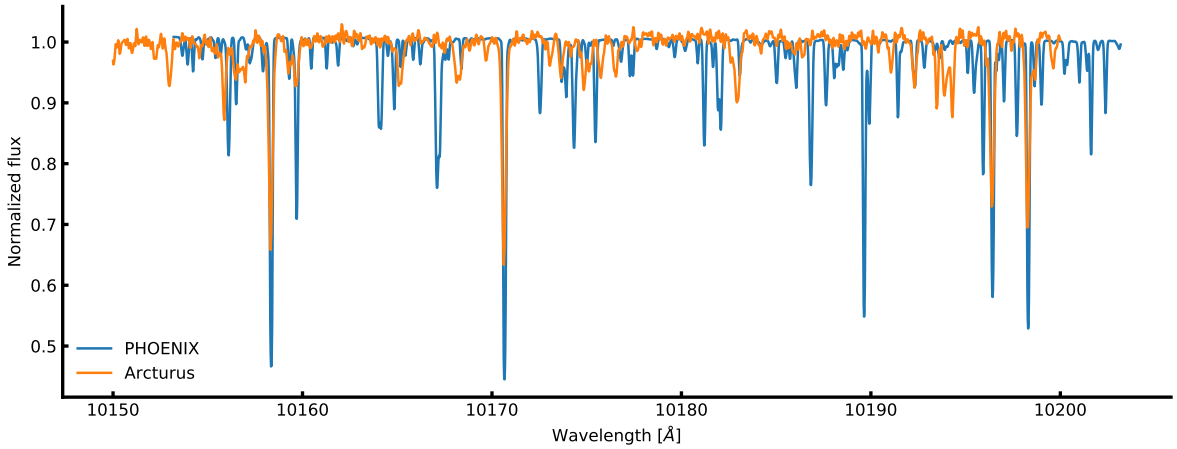

Figure 4.8: Comparison between the Arcturus atlas and a PHOENIX synthetic spectrum with similar parameters to Arcturus (see text for details).

4.6 SWEET-Cat and parameters for 50 planet hosts

The method of determining atmospheric parameters from the curve of growth analysis has been applied several times in the optical (see e.g. Mortier et al., 2013b; Santos et al., 2013; Sousa et al., 2011; Tsantaki et al., 2013). When studying stars with planets and any correlations between stellar and planetary parameters it is important to have a homogeneous characterisation of the stars. An effort to create such a sample was initiated by Santos et al. (2013) with the SWEET-Cat database[5]. The motivation to homogenise the stellar hosts is mainly to compare the hosts and make statistical studies on one consistent scale. When doing these statistical studies, the results might otherwise suffer from offsets between different methods.

The skills acquired during the NIR studies as mentioned above were directly translated into deriving parameters for a sample of 50 known planet host stars that were not previously analysed by our group (Andreasen et al., 2017b). The spectra of these stars were required at UVES, FIES, HARPS, and ESPaDOnS with the mean S/N higher than 200.

Write more about the data acquisition here

[5] https://www.astro.up.pt/resources/sweet-cat/

A Hertzsprung-Russell diagram of the sample can be seen in Figure 4.9. The sample covers a large range of $T_{\rm eff}$, FGK, while there are both dwarf, sub-giant, and some giant stars. The colours indicate the $\log g$. In order to determine the luminosity of each star the simple relation

$$L = 4\pi R^2 \sigma T_{\rm eff}^4$$

is used, where L is the luminosity, R is the stellar radius, and σ is the Stefan-Boltzmann constant. In solar units this relation is simply:

$$\frac{L}{L_\odot} = \left(\frac{R}{R_\odot}\right)^2 \left(\frac{T_{\rm eff}}{T_{\rm eff,\odot}}\right)^4$$

In order to determine the the stellar radius, the empirical relation from Torres et al. (2010) was used.

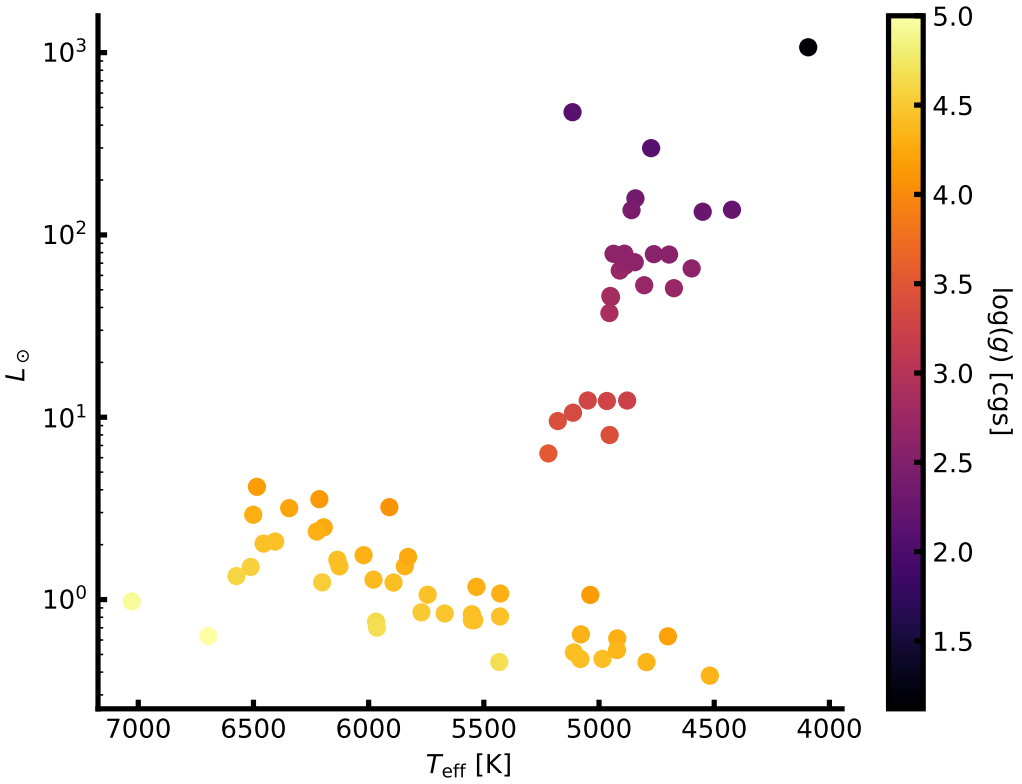

Figure 4.9: A Hertzsprung-Russell diagram of the sample of 50 planet host stars added to SWEET-Cat. The parameters were derived using optical high resolution and high S/N spectra in tandem with `FASMA` and an optical line list. The colour scale shows the derived $\log g$ for each star.

The parameters were derived using `FASMA` with the optical line list compiled by Sousa et al. (2008) and Tsantaki et al. (2013) for stars where $T_{\rm eff}$ was below 5200 K. All the new derived parameters were added to SWEET-Cat, available for the community.

With these updated parameters the completeness of SWEET-Cat for stars brighter than V magnitude

10 is 85% (77% for stars brighter than 12). For fainter stars it is time expensive to acquire spectra of the quality needed for this method. Moreover, many of the fainter planet host stars have been observed with the *Kepler* space mission, where most stars are faint.

SWEET-Cat was recently combined with planetary masses to see two distinctive populations for giant planets by Santos et al. (2017). This can be seen in the mass histogram in Figure 4.10 for the full sample of giant planets, with masses higher than 1 Jupiter mass and lower than 20 Jupiter masses, and for a sample constrained by: $4000\,\mathrm{K} \leq T_{\mathrm{eff}} \leq 6500\,\mathrm{K}$ in order to have reliably atmospheric parameters from spectroscopic data, orbital periods above 10 days to avoid hot jupiters whose formation and migration process is debated (Ngo et al., 2016, see e.g.), orbital periods below 5 years to allow for the sample to be reasonable complete. Last only stars brighter than 13 magnitude were included to ensure that the planetary masses can have been derived with reasonable confidence using the radial velocities.

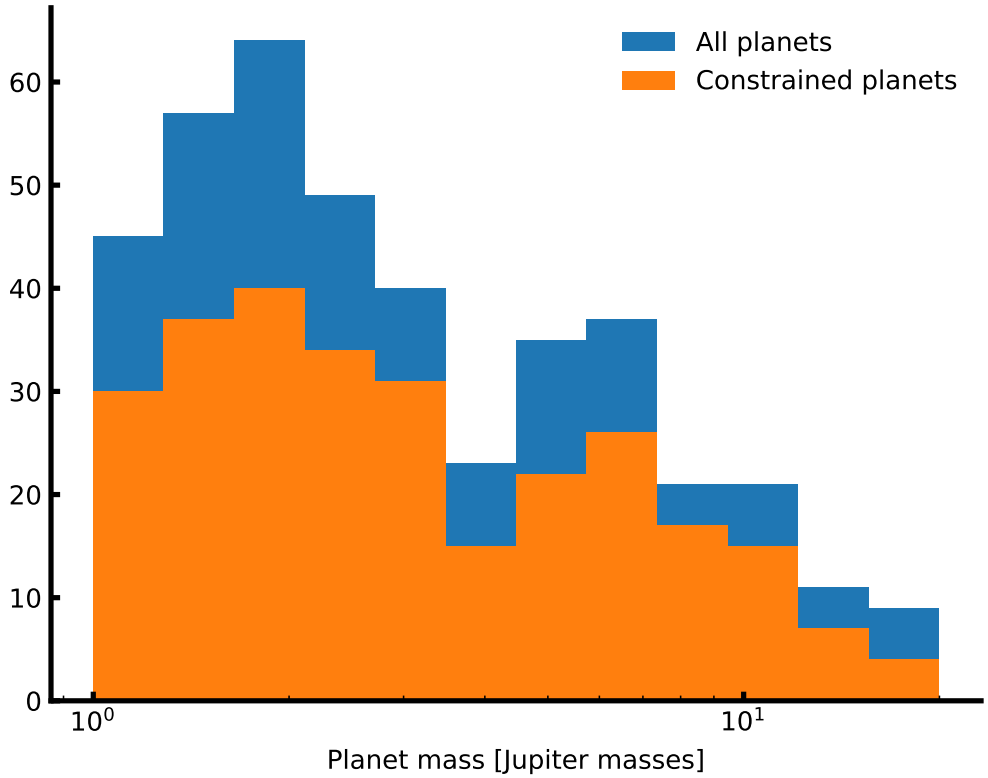

Figure 4.10: Giant planet masses for the full sample and constrained sample (see text for details). This study was performed by Santos et al. (2017) to distinct two giant planet populations.

By separating the distribution into two at $4M_{Jup}$, it can be shown (see Santos et al., 2017, for details) that the stars hosting the more massive giant planets are in average more metal-poor compared to the stars hosting the lower mass giant planets. This suggest two different stellar populations forming giant planets.

4.7 Parameter dependence on EP cut

It is common practise, as in this case, to make a cut in EP for a line list when deriving parameters. This was suggested in Andreasen et al. (2016) (later done in Andreasen et al., 2017a) for the NIR line list used here. This cut was made at 5.5 eV, inspired by a similar cut in the optical (Sousa et al., 2008), including only lines below this limit. The lines with higher EP might also be affected by non-LTE effects which is not treated in this methodology.

As the parameters are dependent on this cut in EP, it seemed interesting to divide a line list in two with upper and lower EPs and analyse those separately. Before going into that analysis it is important to note, that the parameters should not depend on any cut in EP if the theory is right, the radiative transfer code is working properly, and the atmospheric models are correct. Lines with different EP are likely to be formed in different layers of the atmosphere as discussed in Section 2.2, however this should not effect the final derived abundance, which is the problem here.

Make a figure that shows this

Bibliography

Adibekyan, V. Z., Benamati, L., Santos, N. C., Alves, S., Lovis, C., Udry, S., Israelian, G., Sousa, S. G., Tsantaki, M., Mortier, A., Sozzetti, A., and De Medeiros, J. R.: 2015, *MNRAS* **4**50, 1900

Aerts, C., Christensen-Dalsgaard, J., and Kurtz, D. W.: 2010, *Asteroseismology*, Springer-Verlag

Ammler-von Eiff, M., Santos, N. C., Sousa, S. G., Fernandes, J., Guillot, T., Israelian, G., Mayor, M., and Melo, C.: 2009, *A&A* **5**07, 523

Andreasen, D. T., Sousa, S. G., Delgado Mena, E., Santos, N. C., Lebzelter, T., Mucciarelli, A., and Neil, J. J.: 2017a, *A&A* **5**85, A143

Andreasen, D. T., Sousa, S. G., Delgado Mena, E., Santos, N. C., Tsantaki, M., Rojas-Ayala, B., and Neves, V.: 2016, *A&A* **5**85, A143

Andreasen, D. T., Sousa, S. G., Tsantaki, M., Teixeira, G. D. C., Mortier, A., Santos, N. C., Suárez-Andrés, L., Delgado Mena, E., and Ferreira, A. C. S.: 2017b, *A&A* **6**00, A69

Artigau, É., Kouach, D., Donati, J.-F., Doyon, R., Delfosse, X., Baratchart, S., Lacombe, M., Moutou, C., Rabou, P., Parès, L. P., Micheau, Y., Thibault, S., Reshetov, V. A., Dubois, B., Hernandez, O., Vallée, P., Wang, S.-Y., Dolon, F., Pepe, F. A., Bouchy, F., Striebig, N., Hénault, F., Loop, D., Saddlemyer, L., Barrick, G., Vermeulen, T., Dupieux, M., Hébrard, G., Boisse, I., Martioli, E., Alencar, S. H. P., do Nascimento, J.-D., and Figueira, P.: 2014, in *Society of Photo-Optical Instrumentation Engineers (SPIE) Conference Series*, Vol. 9147 of *Society of Photo-Optical Instrumentation Engineers (SPIE) Conference Series*, p. 15

Balachandran, S.: 1990, *ApJ* **3**54, 310

Baraffe, I., Homeier, D., Allard, F., and Chabrier, G.: 2015, *A&A* **5**77, A42

Bedding, T. R., Mosser, B., Huber, D., Montalbán, J., Beck, P., Christensen-Dalsgaard, J., Elsworth, Y. P., García, R. A., Miglio, A., Stello, D., White, T. R., De Ridder, J., Hekker, S., Aerts, C., Barban, C., Belkacem, K., Broomhall, A.-M., Brown, T. M., Buzasi, D. L., Carrier, F., Chaplin, W. J., di Mauro, M. P., Dupret, M.-A., Frandsen, S., Gilliland, R. L., Goupil, M.-J., Jenkins, J. M., Kallinger, T., Kawaler, S., Kjeldsen, H., Mathur, S., Noels, A., Silva Aguirre, V., and Ventura, P.: 2011, *Nature* **4**71, 608

Bensby, T., Feltzing, S., and Oey, M. S.: 2014, *A&A* **5**62, A71

Bertaux, J. L., Lallement, R., Ferron, S., Boonne, C., and Bodichon, R.: 2014, *A&A* **5**64, A46

Blackwell, D. E. and Shallis, M. J.: 1977, *MNRAS* **1**80, 177

Bochanski, J. J., Hawley, S. L., Covey, K. R., West, A. A., Reid, I. N., Golimowski, D. A., and Ivezić, Ž.: 2010, *AJ* **1**39, 2679

Boyajian, T. S., von Braun, K., van Belle, G., McAlister, H. A., ten Brummelaar, T. A., Kane, S. R., Muirhead, P. S., Jones, J., White, R., Schaefer, G., Ciardi, D., Henry, T., López-Morales, M., Ridgway, S., Gies, D., Jao, W.-C., Rojas-Ayala, B., Parks, J. R., Sturmann, L., Sturmann, J., Turner, N. H., Farrington, C., Goldfinger, P. J., and Berger, D. H.: 2012, *ApJ* **7**57, 112

Casagrande, L., Portinari, L., and Flynn, C.: 2006, *MNRAS* **3**73, 13

Casagrande, L., Ramírez, I., Meléndez, J., Bessell, M., and Asplund, M.: 2010, *A&A* **5**12, A54

Cayrel, R.: 1988, in G. Cayrel de Strobel and M. Spite (eds.), *The Impact of Very High S/N Spectroscopy on Stellar Physics*, Vol. 132 of *IAU Symposium*, p. 345

Chaplin, W. J., Kjeldsen, H., Christensen-Dalsgaard, J., Basu, S., Miglio, A., Appourchaux, T., Bedding, T. R., Elsworth, Y., García, R. A., Gilliland, R. L., Girardi, L., Houdek, G., Karoff, C., Kawaler, S. D., Metcalfe, T. S., Molenda-Żakowicz, J., Monteiro, M. J. P. F. G., Thompson, M. J., Verner, G. A., Ballot, J., Bonanno, A., Brandão, I. M., Broomhall, A.-M., Bruntt, H., Campante, T. L., Corsaro, E., Creevey, O. L., Doğan, G., Esch, L., Gai, N., Gaulme, P., Hale, S. J., Handberg, R., Hekker, S., Huber, D., Jiménez, A., Mathur, S., Mazumdar, A., Mosser, B., New, R., Pinsonneault, M. H., Pricopi, D., Quirion, P.-O., Régulo, C., Salabert, D., Serenelli, A. M., Silva Aguirre, V., Sousa, S. G., Stello, D., Stevens, I. R., Suran, M. D., Uytterhoeven, K., White, T. R., Borucki, W. J., Brown, T. M., Jenkins, J. M., Kinemuchi, K., Van Cleve, J., and Klaus, T. C.: 2011, *Science* **3**32, 213

Christensen-Dalsgaard, J., Kjeldsen, H., Brown, T. M., Gilliland, R. L., Arentoft, T., Frandsen, S., Quirion, P.-O., Borucki, W. J., Koch, D., and Jenkins, J. M.: 2010, *ApJL* **7**13, L164

Conod, U., Blind, N., Wildi, F., and Pepe, F.: 2016, in *Society of Photo-Optical Instrumentation Engineers (SPIE) Conference Series*, Vol. 9909 of *Proceedings of the SPIE*, p. 990941

Czekala, I., Andrews, S. M., Mandel, K. S., Hogg, D. W., and Green, G. M.: 2015, *ApJ* **8**12, 128

Delfosse, X., Donati, J.-F., Kouach, D., Hébrard, G., Doyon, R., Artigau, E., Bouchy, F., Boisse, I., Brun, A. S., Hennebelle, P., Widemann, T., Bouvier, J., Bonfils, X., Morin, J., Moutou, C., Pepe, F., Udry, S., do Nascimento, J.-D., Alencar, S. H. P., Castilho, B. V., Martioli, E., Wang, S. Y., Figueira, P., and Santos, N. C.: 2013, in L. Cambresy, F. Martins, E. Nuss, and A. Palacios (eds.), *SF2A-2013: Proceedings of the Annual meeting of the French Society of Astronomy and Astrophysics*, pp 497–508

Dotter, A., Chaboyer, B., Jevremović, D., Kostov, V., Baron, E., and Ferguson, J. W.: 2008, *ApJS* **1**78, 89

Ducati, J. R.: 2002, *VizieR Online Data Catalog* 2237

Favata, F., Micela, G., and Sciortino, S.: 1997, *A&A* **3**23, 809

Follert, R., Dorn, R. J., Oliva, E., Lizon, J. L., Hatzes, A., Piskunov, N., Reiners, A., Seemann, U., Stempels, E., Heiter, U., Marquart, T., Lockhart, M., Anglada-Escude, G., Löwinger, T., Baade, D., Grunhut, J., Bristow, P., Klein, B., Jung, Y., Ives, D. J., Kerber, F., Pozna, E., Paufique, J., Kaeufl, H. U., Origlia, L., Valenti, E., Gojak, D., Hilker, M., Pasquini, L., Smette, A., and Smoker, J.: 2014, in *Society of Photo-Optical Instrumentation Engineers (SPIE) Conference Series*, Vol. 9147 of *Society of Photo-Optical Instrumentation Engineers (SPIE) Conference Series*, p. 19

Girardi, L., Bressan, A., Bertelli, G., and Chiosi, C.: 2000, *A&A Supp.* **1**41, 371

Gonzalez, G., Carlson, M. K., and Tobin, R. W.: 2010, *MNRAS* **4**03, 1368

Gonzalez, G. and Laws, C.: 2000, *AJ* **1**19, 390

Gray, D. F.: 2005, *The Observation and Analysis of Stellar Photospheres, 3rd ed.*

Griffin, R. and Griffin, R.: 1967, *MNRAS* **1**37, 253

Grundahl, F., Fredslund Andersen, M., Christensen-Dalsgaard, J., Antoci, V., Kjeldsen, H., Handberg, R., Houdek, G., Bedding, T. R., Pallé, P. L., Jessen-Hansen, J., Silva Aguirre, V., White, T. R., Frandsen, S., Albrecht, S., Andersen, M. I., Arentoft, T., Brogaard, K., Chaplin, W. J., Harpsøe, K., Jørgensen, U. G., Karovicova, I., Karoff, C., Kjærgaard Rasmussen, P., Lund, M. N., Sloth Lundkvist, M., Skottfelt, J., Norup Sørensen, A., Tronsgaard, R., and Weiss, E.: 2017, *ApJ* **8**36, 142

Gustafsson, B., Edvardsson, B., Eriksson, K., Jørgensen, U. G., Nordlund, Å., and Plez, B.: 2008, *A&A* **4**86, 951

Hinkle, K., Wallace, L., and Livingston, W.: 1995a, *Publications of the ASP* **1**07, 1042

Hinkle, K. H., Wallace, L., and Livingston, W.: 1995b, in A. J. Sauval, R. Blomme, and N. Grevesse (eds.), *Laboratory and Astronomical High Resolution Spectra*, Vol. 81 of *Astronomical Society of the Pacific Conference Series*, p. 66

Huber, D., Silva Aguirre, V., Matthews, J. M., Pinsonneault, M. H., Gaidos, E., García, R. A., Hekker, S., Mathur, S., Mosser, B., Torres, G., Bastien, F. A., Basu, S., Bedding, T. R., Chaplin, W. J., Demory, B.-O., Fleming, S. W., Guo, Z., Mann, A. W., Rowe, J. F., Serenelli, A. M., Smith, M. A., and Stello, D.: 2014, *ApJS* **2**11, 2

Husser, T.-O., Wende-von Berg, S., Dreizler, S., Homeier, D., Reiners, A., Barman, T., and Hauschildt, P. H.: 2013, *A&A* **5**53, A6

Jofré, P., Heiter, U., Soubiran, C., Blanco-Cuaresma, S., Worley, C. C., Pancino, E., Cantat-Gaudin, T., Magrini, L., Bergemann, M., González Hernández, J. I., Hill, V., Lardo, C., de Laverny, P., Lind, K., Masseron, T., Montes, D., Mucciarelli, A., Nordlander, T., Recio Blanco, A., Sobeck, J., Sordo, R., Sousa, S. G., Tabernero, H., Vallenari, A., and Van Eck, S.: 2014, *A&A* **5**64, A133

Kippenhahn, R. and Weigert, A.: 1994, *Stellar Structure and Evolution*, Springer-Verlag

Kjeldsen, H. and Bedding, T. R.: 1995, *A&A* **2**93, 87

Kotani, T., Tamura, M., Suto, H., Nishikawa, J., Sato, B., Aoki, W., Usuda, T., Kurokawa, T., Kashiwagi, K., Nishiyama, S., Ikeda, Y., Hall, D. B., Hodapp, K. W., Hashimoto, J., Morino, J.-I., Okuyama, Y., Tanaka, Y., Suzuki, S., Inoue, S., Kwon, J., Suenaga, T., Oh, D., Baba, H., Narita, N., Kokubo, E., Hayano, Y., Izumiura, H., Kambe, E., Kudo, T., Kusakabe, N., Ikoma, M., Hori, Y., Omiya, M., Genda, H., Fukui, A., Fujii, Y., Guyon, O., Harakawa, H., Hayashi, M., Hidai, M., Hirano, T., Kuzuhara, M., Machida, M., Matsuo, T., Nagata, T., Onuki, H., Ogihara, M., Takami, H., Takato, N., Takahashi, Y. H., Tachinami, C., Terada, H., Kawahara, H., and Yamamuro, T.: 2014, in *Society of Photo-Optical Instrumentation Engineers (SPIE) Conference Series*, Vol. 9147 of *Society of Photo-Optical Instrumentation Engineers (SPIE) Conference Series*, p. 14

Kupka, F. G., Ryabchikova, T. A., Piskunov, N. E., Stempels, H. C., and Weiss, W. W.: 2000, *Baltic Astronomy* **9**, 590

Kurucz, R.: 1993, *ATLAS9 Stellar Atmosphere Programs and 2 km/s grid. Kurucz CD-ROM No. 13. Cambridge, Mass.: Smithsonian Astrophysical Observatory, 1993.* 13

Lebzelter, T., Heiter, U., Abia, C., Eriksson, K., Ireland, M., Neilson, H., Nowotny, W., Maldonado, J., Merle, T., Peterson, R., Plez, B., Short, C. I., Wahlgren, G. M., Worley, C., Aringer, B., Bladh, S., de Laverny, P., Goswami, A., Mora, A., Norris, R. P., Recio-Blanco, A., Scholz, M., Thévenin, F., Tsuji, T., Kordopatis, G., Montesinos, B., and Wing, R. F.: 2012a, *A&A* **5**47, A108

Lebzelter, T., Seifahrt, A., Uttenthaler, S., Ramsay, S., Hartman, H., Nieva, M.-F., Przybilla, N., Smette, A., Wahlgren, G. M., Wolff, B., Hussain, G. A. J., Käufl, H. U., and Seemann, U.: 2012b, *A&A* **5**39, A109

Lindgren, S., Heiter, U., and Seifahrt, A.: 2016, *A&A* **5**86, A100

McWilliam, A.: 1990, *ApJS* **7**4, 1075

Meléndez, J. and Barbuy, B.: 1999, *ApJS* **1**24, 527

Mortier, A., Santos, N. C., Sousa, S., Israelian, G., Mayor, M., and Udry, S.: 2013a, *A&A* **5**51, A112

Mortier, A., Santos, N. C., Sousa, S. G., Adibekyan, V. Z., Delgado Mena, E., Tsantaki, M., Israelian, G., and Mayor, M.: 2013b, *A&A* **5**57, A70

Mucciarelli, A., Pancino, E., Lovisi, L., Ferraro, F. R., and Lapenna, E.: 2013, *ApJ* **7**66, 78

Neuforge-Verheecke, C. and Magain, P.: 1997, *A&A* **3**28, 261

Ngo, H., Knutson, H. A., Hinkley, S., Bryan, M., Crepp, J. R., Batygin, K., Crossfield, I., Hansen, B., Howard, A. W., Johnson, J. A., Mawet, D., Morton, T. D., Muirhead, P. S., and Wang, J.: 2016, *ApJ* **8**27, 8

Nicholls, C. P., Lebzelter, T., Smette, A., Wolff, B., Hartman, H., Käufl, H.-U., Przybilla, N., Ramsay, S., Uttenthaler, S., Wahlgren, G. M., Bagnulo, S., Hussain, G. A. J., Nieva, M.-F., Seemann, U., and Seifahrt, A.: 2017, *A&A* **5**98, A79

Önehag, A., Heiter, U., Gustafsson, B., Piskunov, N., Plez, B., and Reiners, A.: 2012, *A&A* **5**42, A33

Origlia, L., Oliva, E., Baffa, C., Falcini, G., Giani, E., Massi, F., Montegriffo, P., Sanna, N., Scuderi, S., Sozzi, M., Tozzi, A., Carleo, I., Gratton, R., Ghinassi, F., and Lodi, M.: 2014, in *Society of Photo-Optical Instrumentation Engineers (SPIE) Conference Series*, Vol. 9147 of *Society of Photo-Optical Instrumentation Engineers (SPIE) Conference Series*, p. 1

Piskunov, N. E., Kupka, F., Ryabchikova, T. A., Weiss, W. W., and Jeffery, C. S.: 1995, *A&A Supp.* **1**12, 525

Quirrenbach, A., Amado, P. J., Caballero, J. A., Mundt, R., Reiners, A., Ribas, I., Seifert, W., Abril, M., Aceituno, J., Alonso-Floriano, F. J., Ammler-von Eiff, M., Antona Jiménez, R., Anwand-Heerwart, H., Azzaro, M., Bauer, F., Barrado, D., Becerril, S., Béjar, V. J. S., Benítez, D., Berdiñas, Z. M., Cárdenas, M. C., Casal, E., Claret, A., Colomé, J., Cortés-Contreras, M., Czesla, S., Doellinger, M., Dreizler, S., Feiz, C., Fernández, M., Galadí, D., Gálvez-Ortiz, M. C., García-Piquer, A., García-Vargas, M. L., Garrido, R., Gesa, L., Gómez Galera, V., González Álvarez, E., González Hernández, J. I., Grözinger, U., Guàrdia, J., Guenther, E. W., de Guindos, E., Gutiérrez-Soto, J., Hagen, H.-J., Hatzes, A. P., Hauschildt, P. H., Helmling, J., Henning, T., Hermann, D., Hernández Castaño, L., Herrero, E., Hidalgo, D., Holgado, G., Huber, A., Huber, K. F., Jeffers, S., Joergens, V., de Juan, E., Kehr, M., Klein, R., Kürster, M., Lamert, A., Lalitha, S., Laun, W., Lemke, U., Lenzen, R., López del Fresno, M., López Martí, B., López-Santiago, J., Mall, U., Mandel, H., Martín, E. L., Martín-Ruiz, S., Martínez-Rodríguez, H., Marvin, C. J., Mathar, R. J., Mirabet, E., Montes, D., Morales Muñoz, R., Moya, A., Naranjo, V., Ofir, A., Oreiro, R., Pallé, E., Panduro, J., Passegger, V.-M., Pérez-Calpena, A., Pérez Medialdea, D., Perger, M., Pluto, M., Ramón, A., Rebolo, R., Redondo, P., Reffert, S., Reinhardt, S., Rhode, P., Rix, H.-W., Rodler, F., Rodríguez, E., Rodríguez-López, C., Rodríguez-Pérez, E., Rohloff, R.-R., Rosich, A., Sánchez-Blanco, E., Sánchez Carrasco, M. A., Sanz-Forcada, J., Sarmiento, L. F., Schäfer, S., Schiller, J., Schmidt, C., Schmitt, J. H. M. M., Solano, E., Stahl, O., Storz, C., Stürmer, J., Suárez, J. C., Ulbrich, R. G., Veredas, G., Wagner, K., Winkler, J., Zapatero Osorio, M. R., Zechmeister, M., Abellán de Paco, F. J., Anglada-Escudé, G., del Burgo, C., Klutsch, A., Lizon, J. L., López-Morales, M., Morales, J. C., Perryman, M. A. C., Tulloch, S. M., and Xu, W.: 2014, in *Society of Photo-Optical Instrumentation Engineers (SPIE) Conference Series*, Vol. 9147 of *Society of Photo-Optical Instrumentation Engineers (SPIE) Conference Series*, p. 1

Ramírez, I., Allende Prieto, C., and Lambert, D. L.: 2013, *ApJ* **7**64, 78

Ramírez, I., Fish, J. R., Lambert, D. L., and Allende Prieto, C.: 2012, *ApJ* **7**56, 46

Ramírez, I. and Meléndez, J.: 2005a, *ApJ* **6**26, 446

Ramírez, I. and Meléndez, J.: 2005b, *ApJ* **6**26, 465

Rayner, J., Bond, T., Bonnet, M., Jaffe, D., Muller, G., and Tokunaga, A.: 2012, in *Ground-based and Airborne Instrumentation for Astronomy IV*, Vol. 8446 of *Proceedings of the SPIE*, p. 84462C

Rayner, J., Tokunaga, A., Jaffe, D., Bonnet, M., Ching, G., Connelley, M., Kokubun, D., Lockhart, C., and Warmbier, E.: 2016, in *Society of Photo-Optical Instrumentation Engineers (SPIE) Conference Series*, Vol. 9908 of *Proceedings of the SPIE*, p. 990884

Recio-Blanco, A., Bijaoui, A., and de Laverny, P.: 2006, *MNRAS* **3**70, 141

Santos, N. C., Adibekyan, V., Figueira, P., Andreasen, D. T., Barros, S. C. C., Delgado-Mena, E., Demangeon, O., Faria, J. P., Oshagh, M., Sousa, S. G., Viana, P. T. P., and Ferreira, A. C. S.: 2017, *ArXiv e-prints*

Santos, N. C., Israelian, G., and Mayor, M.: 2004, *A&A* **4**15, 1153

Santos, N. C., Sousa, S. G., Mortier, A., Neves, V., Adibekyan, V., Tsantaki, M., Delgado Mena, E., Bonfils, X., Israelian, G., Mayor, M., and Udry, S.: 2013, *A&A* **5**56, A150

Smiljanic, R., Korn, A. J., Bergemann, M., Frasca, A., Magrini, L., Masseron, T., Pancino, E., Ruchti, G., San Roman, I., Sbordone, L., Sousa, S. G., Tabernero, H., Tautvaišienė, G., Valentini, M., Weber, M., Worley, C. C., Adibekyan, V. Z., Allende Prieto, C., Barisevičius, G., Biazzo, K., Blanco-Cuaresma, S., Bonifacio, P., Bragaglia, A., Caffau, E., Cantat-Gaudin, T., Chorniy, Y., de Laverny, P., Delgado-Mena, E., Donati, P., Duffau, S., Franciosini, E., Friel, E., Geisler, D., González Hernández, J. I., Gruyters, P., Guiglion, G., Hansen, C. J., Heiter, U., Hill, V., Jacobson, H. R., Jofre, P., Jönsson, H., Lanzafame, A. C., Lardo, C., Ludwig, H.-G., Maiorca, E., Mikolaitis, Š., Montes, D., Morel, T., Mucciarelli, A., Muñoz, C., Nordlander, T., Pasquini, L., Puzeras, E., Recio-Blanco, A., Ryde, N., Sacco, G., Santos, N. C., Serenelli, A. M., Sordo, R., Soubiran, C., Spina, L., Steffen, M., Vallenari, A., Van Eck, S., Villanova, S., Gilmore, G., Randich, S., Asplund, M., Binney, J., Drew, J., Feltzing, S., Ferguson, A., Jeffries, R., Micela, G., Negueruela, I., Prusti, T., Rix, H.-W., Alfaro, E., Babusiaux, C., Bensby, T., Blomme, R., Flaccomio, E., François, P., Irwin, M., Koposov, S., Walton, N., Bayo, A., Carraro, G., Costado, M. T., Damiani, F., Edvardsson, B., Hourihane, A., Jackson, R., Lewis, J., Lind, K., Marconi, G., Martayan, C., Monaco, L., Morbidelli, L., Prisinzano, L., and Zaggia, S.: 2014, *A&A* **5**70, A122

Sneden, C. A.: 1973, *Ph.D. thesis*, THE UNIVERSITY OF TEXAS AT AUSTIN.

Soubiran, C., Le Campion, J.-F., Brouillet, N., and Chemin, L.: 2016, *A&A* **5**91, A118

Sousa, S. G., Santos, N. C., Adibekyan, V., Delgado-Mena, E., and Israelian, G.: 2015, *A&A* **5**77, A67

Sousa, S. G., Santos, N. C., Israelian, G., Mayor, M., and Monteiro, M. J. P. F. G.: 2007, *A&A* **4**69, 783

Sousa, S. G., Santos, N. C., Israelian, G., Mayor, M., and Udry, S.: 2011, *A&A* **5**33, A141

Sousa, S. G., Santos, N. C., Mayor, M., Udry, S., Casagrande, L., Israelian, G., Pepe, F., Queloz, D., and Monteiro, M. J. P. F. G.: 2008, *A&A* **4**87, 373

Torres, G., Andersen, J., and Giménez, A.: 2010, *Astronomy and Astrophysics Reviews* **1**8, 67

Torres, G., Fischer, D. A., Sozzetti, A., Buchhave, L. A., Winn, J. N., Holman, M. J., and Carter, J. A.: 2012, *ApJ* **7**57, 161

Torres, G., Winn, J. N., and Holman, M. J.: 2008, *ApJ* **6**77, 1324

Tsantaki, M., Andreasen, D. T., Teixeira, G. D. C., Sousa, S. G., Santos, N. C., Delgado-Mena, E., and Bruzual, G.: 2017, *MNRAS* **5**55, A150

Tsantaki, M., Sousa, S. G., Adibekyan, V. Z., Santos, N. C., Mortier, A., and Israelian, G.: 2013, *A&A* **5**55, A150

Tsantaki, M., Sousa, S. G., Santos, N. C., Montalto, M., Delgado-Mena, E., Mortier, A., Adibekyan, V., and Israelian, G.: 2014, *A&A* **57**0, A80

Valenti, J. A. and Fischer, D. A.: 2005, *ApJS* **1**59, 141

Valenti, J. A. and Piskunov, N.: 1996, *A&A Supp.* **1**18, 595